

CHITOSAN/ZINC-IRON OXIDE NANOCOMPOSITE FOR CONTROLLED  
RELEASE OF ANTICANCER DRUG IMATINIB

MERVE ECE TEMELKURAN, ZEYNEP KALAYCIOĞLU and FATMA BEDIA ERİM

*Department of Chemistry, Faculty of Science and Letters, Istanbul Technical University,  
Maslak, Istanbul, Turkey*✉ *Corresponding authors: F. Bedia Erim, erim@itu.edu.tr**Z. Kalaycioğlu, kalayciogluz@itu.edu.tr**Received June 27, 2024*

Cancer drug carriers at the nanoparticle level have gained significant importance in recent years due to their ability to enhance the delivery of active substances to cancer tissues, thereby improving efficacy and reducing negative side effects associated with traditional chemotherapy. In this study, chitosan nanoparticles were synthesized and coated with zinc-iron oxide nanoparticles. This approach offers the advantage of targeted drug delivery to tumors. Imatinib, an anticancer drug, was loaded into both chitosan nanoparticles and chitosan/zinc-iron oxide nanoparticles. The addition of zinc-iron oxide nanoparticles significantly increased the encapsulation efficiency of the chitosan-based nanoparticles from 36% to 77.8%. The chitosan/zinc-iron oxide nanoparticle system was selected as the drug delivery system and characterized using Fourier transform infrared spectroscopy, scanning electron microscopy, and energy-dispersive X-ray spectroscopy, and X-ray diffraction techniques. *In-vitro* release studies demonstrated sustained release of imatinib. These findings suggest that the chitosan/zinc-iron oxide nanoparticles hold promise as an effective drug delivery system for cancer therapy.

**Keywords:** biopolymeric nanoparticles, cancer, drug delivery

**INTRODUCTION**

Cancer is a significant global public health issue, and its treatment has always been challenging. The increasing rate of patients with different types of cancer has raised the alarm about a potential health concern. An estimated 28 million new cancer cases will be recorded annually by 2040, if incidence remains unchanged and population growth and aging follow current trends.<sup>1</sup> Various cancer treatment strategies, such as chemotherapy and radiation therapy, have been used to reduce the increasing cancer rate.<sup>2</sup> However, these conventional methods often lack site-specificity and may require long-term drug use, leading to adverse side effects. Therefore, there is a pressing need for more effective techniques in cancer treatment.

Nanocarrier-based drug delivery systems and nanoparticles are one of the promising approaches in cancer therapy.<sup>3,4</sup> These systems offer the potential for targeted delivery of therapeutic agents to cancerous tissues.

Nanoparticles based on polysaccharides have received significant attention in recent years since

they are physiologically stable, biocompatible, biodegradable, and non-toxic.<sup>5,6</sup> Among them, chitosan nanoparticles are widely used due to the chitosan's advantageous features, which include enhanced biodistribution, specificity, sensitivity, and minimal toxicity on normal cells.<sup>7</sup> Chitosan-based nanoformulations have gained attention in controlled release systems due to their high loading capacity.<sup>8</sup> Anti-inflammatory drugs, antibiotics, anticancer drugs, and antidiabetic compounds were successfully loaded into chitosan-based nanocarriers.<sup>9-12</sup> The application of chitosan nanocarriers in breast, prostate, and colon cancer has been reported by researchers.<sup>13-16</sup> Khalaf *et al.* (2023) reviewed the potential biomedical and clinical applications of chitosan nanocarriers as new-generation materials for the future.<sup>17</sup> Composite nanomaterials obtained by combining different nanoparticles increase efficiency in applications.<sup>18-21</sup> Furthermore, integrating nanoparticles with biopolymers has improved photocatalytic activity, adsorption capacity,

antibacterial activity, and mechanical properties, as demonstrated in previous studies.<sup>22-25</sup>

Iron oxide nanoparticles are the only nanoparticles approved by the Food and Drug Administration (FDA) and the European Medicines Agency (EMA).<sup>26</sup> They have garnered significant attention in various medical fields.<sup>27,28</sup> Their adequate size and shape tuning, which can imitate particular biological entities like proteins, genes, viruses, and cells, is the main draw of these nanoparticles. Bimetallic magnetic nanoparticles have also been developed in addition to iron oxide nanoparticles. Zinc has been reported as a biocompatible dopant for magnetic iron oxide nanoparticles.<sup>26</sup>

Imatinib mesylate is the first successful member of kinase inhibitors that functions by specifically inhibiting tyrosine kinases in chronic myeloid leukemia (CML).<sup>29</sup> In addition, it inhibits the activation of platelet-derived growth factor (PDGF) and colony-stimulating factor 1 (CSF1) receptors, which regulate key cellular processes. Imatinib is currently used in research and the treatment of various solid tumors.<sup>30,31</sup> However, the bioavailability of imatinib under physiological conditions is significantly limited due to its hydrophobic nature. To address this limitation, advanced drug delivery systems are required to ensure that the drug reaches the target site in adequate concentrations.<sup>32</sup> Our study aimed to leverage the biocompatibility and non-toxicity of chitosan along with the superparamagnetic properties of zinc-iron oxide in the context of a cancer drug delivery system. Chitosan nanoparticles were synthesized and doped with zinc-iron oxide nanoparticles. To enhance the therapeutic potential of the chemotherapeutic agent imatinib (Gleevec), the drug was loaded onto chitosan/zinc-iron oxide nanoparticles. Imatinib has been previously loaded onto various nanoparticles, including poly-electrolytic lithium nanocapsules,<sup>33</sup> PVP-modified gold nanoparticles,<sup>34</sup> starch carbon quantum dots,<sup>35</sup> silver nanoparticles,<sup>36</sup> Fe<sub>3</sub>O<sub>4</sub>-alginate nanoparticles,<sup>37</sup> and Fe<sub>3</sub>O<sub>4</sub>-chitosan nanoparticles.<sup>38,39</sup>

To our knowledge, this study represents the first synthesis and characterization of chitosan/zinc-iron oxide nanocomposites. Additionally, it is the first investigation into the encapsulation of imatinib within these particles and the study of its controlled release.

## EXPERIMENTAL

### Materials

Low molecular weight chitosan obtained from crab shells, with a minimum deacetylation degree of 85%, sodium tripolyphosphate (85% purity), glacial acetic acid, and zinc-iron oxide nanoparticles (ZnFe<sub>2</sub>O<sub>4</sub> NPs) (particle size (BET) <100 nm and >99% purity), cellulose dialysis membranes were bought from Sigma-Aldrich (Germany). Tween 80, disodium hydrogen phosphate heptahydrate (Na<sub>2</sub>HPO<sub>4</sub>·7H<sub>2</sub>O), sodium dihydrogen phosphate dihydrate (NaH<sub>2</sub>PO<sub>4</sub>·2H<sub>2</sub>O), sodium chloride (NaCl), and sodium hydroxide (NaOH) were purchased from Merck (Germany). Imatinib mesylate powder (>99% purity), (IUPAC name: methanesulfonic acid; 4-[(4-methylpiperazin-1-yl)methyl]-N-[4-methyl-3-[(4-pyridin-3-yl)pyrimidin-2-yl)amino]phenyl]benzamide) was generously gifted by Novartis, Türkiye.

### Preparation of chitosan nanoparticles

Chitosan nanoparticles (NPs) were prepared using an ionic gelation technique developed by Calvo *et al.* (1997), with minor modification.<sup>40</sup> Briefly, 0.4 g of chitosan was weighed and dissolved in 100 mL of 1% aqueous acetic acid under magnetic stirring at room temperature for 12 hours. 0.2 g of sodium tripolyphosphate (Na-TPP) was dissolved in distilled water (100 mL). The TPP solution was added dropwise into the chitosan solution under constant stirring at room temperature. The mixture was stirred at 500 rpm for 1 hour after the complete addition of TPP. The resulting turbid solution contains chitosan NPs. The mixture was centrifuged at 13000 rpm for 20 minutes (Sigma 2-16P, Germany), which was continued by discarding the supernatant. The residue was washed several times with ethanol/deionized water. Eventually, it was dried overnight at 1 bar and -50 °C in a lyophilizer.

### Preparation of chitosan/ZnFe<sub>2</sub>O<sub>4</sub> nanocomposite

ZnFe<sub>2</sub>O<sub>4</sub> NPs were conjugated to chitosan NPs according to the following approach for synthesizing chitosan/ZnFe<sub>2</sub>O<sub>4</sub> nanocomposite. Briefly, 100 mg of ZnFe<sub>2</sub>O<sub>4</sub> NPs were weighed and dispersed in 5 mL of 1% (v/v) Tween 80 solution using a homogenizer for 10 min at room temperature. Next, the dispersion of ZnFe<sub>2</sub>O<sub>4</sub> NPs was mixed with 5 mL of 4 mg/mL chitosan solution under stirring at 500 rpm and room temperature for one h. Then, TPP solution was added dropwise to this solution and centrifugation was performed at 13000 rpm for 20 minutes. The residue was washed several times with ethanol/distilled water, then dried overnight at 1 bar and -50 °C in the lyophilizer.

### Preparation of imatinib encapsulated chitosan/ZnFe<sub>2</sub>O<sub>4</sub> nanocomposites

To encapsulate the imatinib drug, 3 mg of imatinib was dissolved in 10 mL of methanol-ethanol solution and added to the chitosan/ZnFe<sub>2</sub>O<sub>4</sub> dispersion in the

methanol-ethanol solution. Then, the same procedure was applied for the nanoparticle preparation. After gelation with TPP was performed, the mixture was stirred for one hour at room temperature. The resultant solid was separated using a centrifuge (1300 rpm, 20 min), washed with ethanol/distilled water, and dried in the lyophilizer to obtain the final chitosan/ZnFe<sub>2</sub>O<sub>4</sub>/imatinib nanoparticles.

The chemical structure of imatinib and the synthesis procedures of chitosan/ZnFe<sub>2</sub>O<sub>4</sub> and imatinib-loaded chitosan/ZnFe<sub>2</sub>O<sub>4</sub> nanocomposite are presented in Figure 1.

### Encapsulation efficiency

The chitosan/ZnFe<sub>2</sub>O<sub>4</sub>/imatinib nanocomposite supernatant was separated to determine the encapsulation efficiency. The imatinib content of the supernatant was estimated by measuring its absorbance at 266 nm. At this wavelength, absorbance measurements were recorded for imatinib mesylate at a concentration range of 2-15 mg/L, and a standard calibration curve was drawn. Imatinib concentration was calculated from the calibration curve equation. After that, the encapsulation efficiency (EE) as a percent was calculated using Equation (1):

$$EE (\%) = \frac{\text{Total imatinib concentration} - \text{Free imatinib concentration}}{\text{Total imatinib concentration}} \times 100 \quad (1)$$

where total imatinib concentration refers to the amount of imatinib added to the medium during the chitosan/ZnFe<sub>2</sub>O<sub>4</sub>/imatinib nanocomposite preparation

process, and free imatinib refers to the amount of imatinib remaining in the supernatant separated from the solid phase after the nanoparticles precipitate.

### Characterization of the prepared nanocomposite

The structural properties of the chitosan NPs, chitosan/ZnFe<sub>2</sub>O<sub>4</sub> nanocomposite, and chitosan/ZnFe<sub>2</sub>O<sub>4</sub>/imatinib nanocomposite were analyzed by Fourier transform infrared (FTIR) spectroscopy using a single reflectance ATR cell by accumulating 64 scans with a resolution of 4.0 cm<sup>-1</sup>. All data were recorded in the 4000–400 cm<sup>-1</sup> spectral range.

The particle morphology of the chitosan/ZnFe<sub>2</sub>O<sub>4</sub> nanocomposite was investigated using an LEO Supra VP 35 field emission scanning electron microscope (FE-SEM) system.

To verify the ZnFe<sub>2</sub>O<sub>4</sub> crystalline phase, X-ray diffraction (XRD) analysis was performed. The XRD patterns were determined by a Philips X'Pert Pro powder diffractometer (Eindhoven, Netherlands) using Cu K $\alpha$  radiation ( $\lambda = 1.5418 \text{ \AA}$ , 40 kV, 40 mA).

The point of zero charge (PZC) value of the ZnFe<sub>2</sub>O<sub>4</sub> NPs and chitosan/ZnFe<sub>2</sub>O<sub>4</sub> nanocomposite was determined by the pH drift method.<sup>41</sup> The pH of the 0.1 mol L<sup>-1</sup> NaNO<sub>3</sub> was adjusted to a value between 2 and 12 using 0.1 mol L<sup>-1</sup> HCl or 0.1 mol L<sup>-1</sup> NaOH. Each type of nanoparticles (0.1 g) was added to 20 mL of the pH-adjusted solution in a capped vial, separately. The vials were shaken up in a shaker and equilibrated for 24 h. The final pH was measured and plotted against the initial pH. The pH at which the curve crosses the pH<sub>initial</sub> = pH<sub>final</sub> line was taken as the PZC.

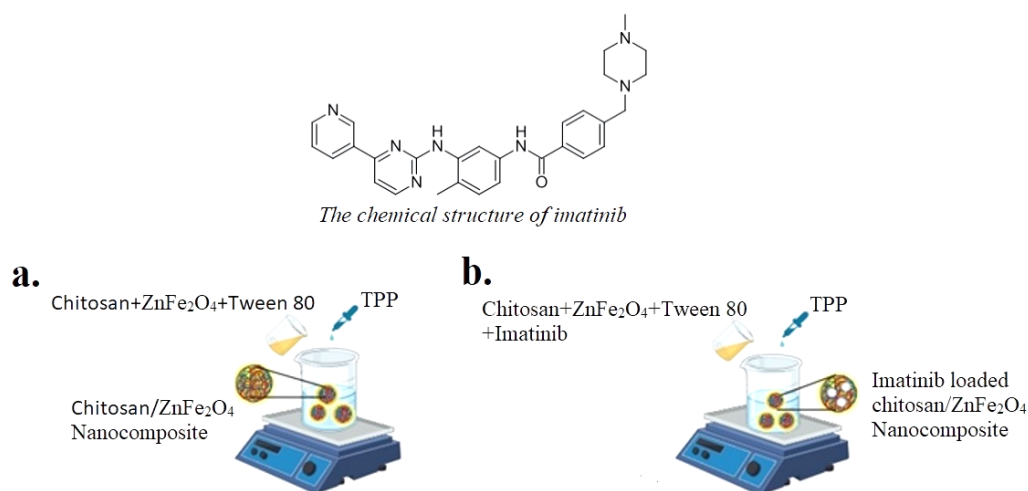


Figure 1: Synthesis procedure of (a) chitosan/ZnFe<sub>2</sub>O<sub>4</sub> and (b) chitosan/ZnFe<sub>2</sub>O<sub>4</sub>/imatinib nanocomposites

### In vitro imatinib release from chitosan/ZnFe<sub>2</sub>O<sub>4</sub>/imatinib nanocomposite

The chitosan/ZnFe<sub>2</sub>O<sub>4</sub>/imatinib nanocomposite was weighed as 3 mg, added into 10 mL of 0.1 mol L<sup>-1</sup> phosphate buffered saline solution (pH=7.4), and sonicated for 5 min. The dispersion was transferred into a dialysis tube with a molecular cutoff of 14000 Da and

dipped into 25 mL of a 0.1 M phosphate-buffered saline solution (PBS, pH=7.4). The solution was stirred at 37 °C and 100 rpm. The solution containing the released imatinib drug was withdrawn every 5 minutes during the first half hour and every 30 minutes at the end. Its imatinib content was measured by monitoring the absorbance at 266 nm. The collected solution was then

mixed with an equal volume of PBS. The drug release assay was performed in triplicate.

**Analysis of the *in vitro* release kinetics**

The zero-order (Eq. 2), first-order (Eq. 3), Higuchi (Eq. 4), and Korsmeyer-Peppas (Eq. 5) kinetic models were used to evaluate the *in vitro* drug release:

$$Q_t = Q_0 + k_0 t \tag{2}$$

$$\log Q_t = \log Q_0 - k_1 t / 2.303 \tag{3}$$

$$Q_t = k_H t^{1/2} \tag{4}$$

$$M_t / M_\infty = k t^n \tag{5}$$

where  $Q_t$  is the concentration of drug (mol/L) released at time  $t$ ,  $Q_0$  is the initial concentration of drug in solution,  $k_0$  is the zero-order release constant (expressed as concentration/time), the constant  $k_1$  is first order (expressed in time units,  $\text{min}^{-1}$ ),  $k_H t^{1/2}$  is the dissolution constant of the Higuchi equation (expressed in time units,  $\text{min}^{1/2}$ ),  $M_t$  is the amount of drug released at time  $t$ ,  $M_\infty$  is the total amount of drug released at infinite time,  $k$  is the release rate constant (expressed as  $\text{min}^{-n}$ ) and  $n$  is the release exponent, which indicates the type of release mechanism.

**RESULTS AND DISCUSSION**

**Process yield of chitosan NPs and chitosan/ZnFe<sub>2</sub>O<sub>4</sub> nanocomposite**

The optimal conditions for chitosan NPs were found by trying the various formulations and calculating the process yield. The effect of

formulation variables, such as chitosan and TPP concentration, on process yield was examined. Mixing time was chosen as a process variable. In the experiments conducted for a selected parameter, all other parameters were kept constant. While investigating the effect of chitosan concentration on the reaction yield, the TPP concentration was kept constant at 2.0 mg mL<sup>-1</sup>, and the chitosan concentration was varied at 2.0, 3.0, and 4.0 mg mL<sup>-1</sup>. The solution obtained after 60 minutes of mixing was subjected to centrifugation and lyophilization. Finally, the percentage process yield was calculated using the equation below:

$$\text{Process yield (\%)} = \frac{\text{weight of nanoparticles formed}}{\text{total amount of substance}} \tag{6}$$

The percentage yields of the various nanoparticle formulations are presented in Table 1. It was observed that the highest efficiency was obtained with 4.0 mg mL<sup>-1</sup> chitosan.

Optimization of TPP concentration was carried out by selecting chitosan concentration of 4.0 mg mL<sup>-1</sup> and a mixing time of 60 min. Under these conditions, nanoparticles were produced by changing the concentration of TPP between 1.0 and 4.0 mg mL<sup>-1</sup>. The highest reaction yield was obtained with 2.0 mg mL<sup>-1</sup>.

Table 1  
Optimization of chitosan NPs

Formulation No.	Chitosan concentration (mg mL <sup>-1</sup> )	TPP concentration (mg mL <sup>-1</sup> )	Stirring time (min)	Yield (%)
1	4.0	2.0	60	42
2	3.0	2.0	60	37
3	2.0	2.0	60	22
4	4.0	3.0	60	25
5	4.0	1.5	60	13
6	4.0	1.0	30	10
7	4.0	2.0	30	32
8	4.0	2.0	90	38

Finally, the optimization of magnetic stirring time was carried out. The chitosan and TPP concentrations were kept constant at 4.0 mg mL<sup>-1</sup> and 2.0 mg mL<sup>-1</sup>, respectively. The mixing time was varied as 30, 60, and 90 min. The highest reaction yield (42%) was obtained with a stirring time of 60 min.

To optimize the amount of ZnFe<sub>2</sub>O<sub>4</sub>, 10, 50, and 100 mg particles were weighed and conjugated to the chitosan NPs, as described in the experimental section. The yield of completely dried chitosan/ZnFe<sub>2</sub>O<sub>4</sub> nanocomposite was calculated.

The highest reaction efficiency (52%) was obtained with 100 mg ZnFe<sub>2</sub>O<sub>4</sub>.

**Characterization of the chitosan/ZnFe<sub>2</sub>O<sub>4</sub> nanocomposite**

The FTIR spectra of chitosan, chitosan NPs, chitosan/ZnFe<sub>2</sub>O<sub>4</sub> nanocomposite, and chitosan/ZnFe<sub>2</sub>O<sub>4</sub>/imatinib nanocomposite are given in Figure 2. The FTIR spectrum of imatinib (Fig. 2a) shows multiple peaks between 1724 cm<sup>-1</sup> – 409 cm<sup>-1</sup>. These peaks were observed at 2988 cm<sup>-1</sup> (C–H bending), 1724 cm<sup>-1</sup> (C=O band), 1557, and

1363  $\text{cm}^{-1}$  (aromatic C=C, C=N stretching vibration, respectively), 1286  $\text{cm}^{-1}$  (C–N stretching vibration), 1136  $\text{cm}^{-1}$  (C–O stretching vibration), and 878  $\text{cm}^{-1}$  (out-of-plane aromatic C–H deformations), which was compatible with the study of Jalabubu *et al.* (2018).<sup>41</sup> These peaks were also present in the FTIR spectrum of the chitosan/ZnFe<sub>2</sub>O<sub>4</sub>/imatinib nanocomposite (Fig. 2b), which means it was physically entrapped into the nanocomposite. The FTIR spectrum of the chitosan/ZnFe<sub>2</sub>O<sub>4</sub>/imatinib nanocomposite also showed a strong band in the region 3610–3180  $\text{cm}^{-1}$  corresponding to the N–H stretching of chitosan. Imatinib mesylate is a molecule that

shows polymorphism, and drug components can consist of polymorphic mixtures.<sup>42</sup> Lin *et al.* (2019) reported polymorphic transformation from  $\alpha$ -form to  $\beta$ -form in methanol solution.<sup>43</sup> Szczepek *et al.* (2010) showed that the peaks that appeared in the  $\alpha$ -form in the IR band between 2706–2492  $\text{cm}^{-1}$  disappeared in the  $\beta$ -form.<sup>44</sup> Therefore, the peaks that are not visible in Figure 1a and appear in Figure 1b in the range 2494–2600  $\text{cm}^{-1}$  show the polymorphic transformation of imatinib in the composite preparation process. Figure 2c and Figure 2d present the FTIR spectra of chitosan NPs and chitosan/ZnFe<sub>2</sub>O<sub>4</sub> nanocomposite, respectively.

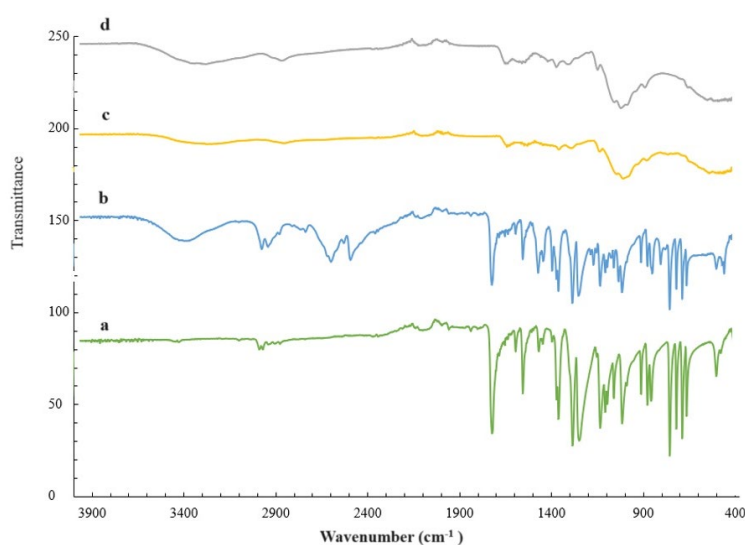


Figure 2: FTIR spectra of (a) pure imatinib, (b) chitosan/ZnFe<sub>2</sub>O<sub>4</sub>/imatinib nanocomposite, (c) chitosan nanoparticles, (d) chitosan/ZnFe<sub>2</sub>O<sub>4</sub> nanocomposite

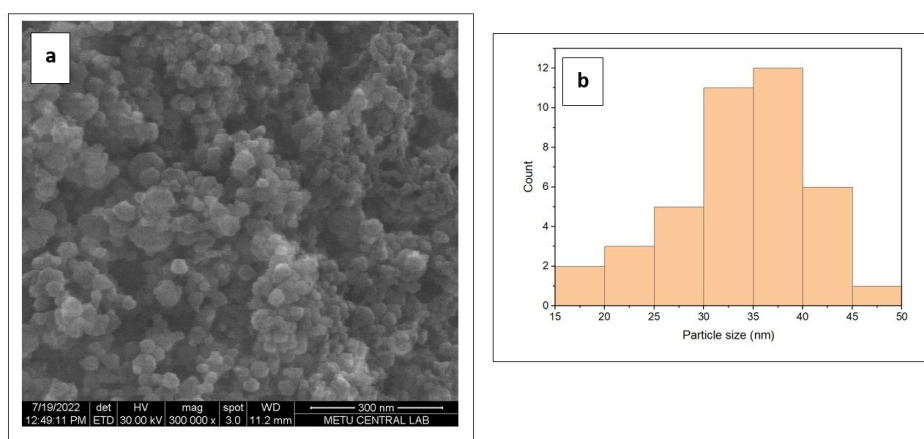


Figure 3: (a) SEM image and (b) Particle size distribution histogram of chitosan/ZnFe<sub>2</sub>O<sub>4</sub> nanocomposite

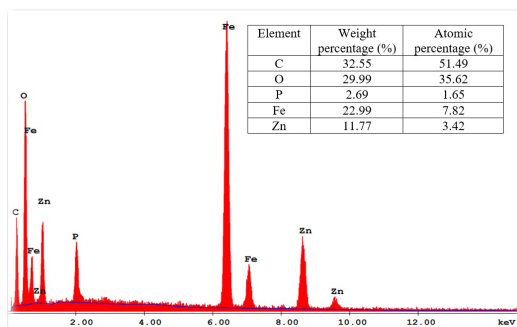


Figure 4: EDX analysis of chitosan/ZnFe<sub>2</sub>O<sub>4</sub> nanocomposite

FESEM evaluated the size and morphology of the chitosan/ZnFe<sub>2</sub>O<sub>4</sub> nanocomposite. The FESEM image of chitosan/ZnFe<sub>2</sub>O<sub>4</sub> nanocomposite is shown in Figure 3a. As seen in Figure 3a, chitosan/ZnFe<sub>2</sub>O<sub>4</sub> nanocomposite is spherical and the size distribution is monodisperse. The radius values of 40 spherical particles in the image were analyzed using ImageJ 1.52a software. The average particle size was calculated as 35 nm. The histogram of the size distribution is given in Figure 3b. Nanocomposites with a diameter of less than 100 nm have been identified as ideal for targeted therapeutic administration at cancer sites, as they can be efficiently distributed within the capillaries of cancerous tissues.<sup>45</sup>

Moreover, SEM-EDX analysis was performed to show the existence of chitosan shell and ZnFe<sub>2</sub>O<sub>4</sub> on the surface of the nanocomposite. The results confirmed the presence of Fe, C, N, O, Zn, and P in Figure 4. The percentages of each element are given on the graph.

Figure 5 shows the XRD pattern of commercial ZnFe<sub>2</sub>O<sub>4</sub> NPs and the synthesized chitosan/ZnFe<sub>2</sub>O<sub>4</sub> nanocomposite. ZnFe<sub>2</sub>O<sub>4</sub> NPs were identified by indexing the peaks with JCPDS No. 22-1012. There is consistency between the diffractograms of the synthesized chitosan/ZnFe<sub>2</sub>O<sub>4</sub> nanocomposite (Fig. 5a) and the ZnFe<sub>2</sub>O<sub>4</sub> NPs (Fig. 5b). The presence of ZnFe<sub>2</sub>O<sub>4</sub> NPs in the nanocomposite is confirmed by the characteristic peaks at two theta (2θ) values of approximately 29.9, 35.3, 43.1, 56.8, 62.2°. These peaks correspond to the (220), (311), (400), (511), and (440) Bragg reflections of the cubic spinel structure, respectively. The XRD spectrum of chitosan/ZnFe<sub>2</sub>O<sub>4</sub> nanocomposite also shows a broad band at 2θ=20°, indicating an amorphous structure of chitosan inclusion.

The point of the zero charge of commercial ZnFe<sub>2</sub>O<sub>4</sub> NPs was determined at pH 8.0 and chitosan/ZnFe<sub>2</sub>O<sub>4</sub> nanocomposite at pH 6.5.

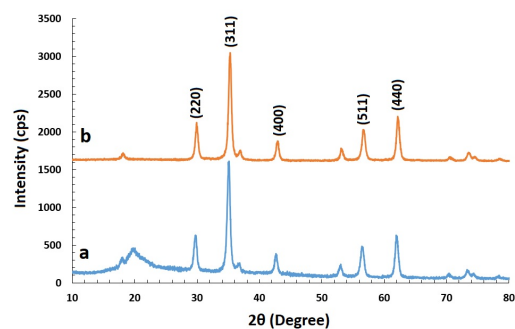


Figure 5: XRD spectra of (a) chitosan/ZnFe<sub>2</sub>O<sub>4</sub> nanocomposite and (b) ZnFe<sub>2</sub>O<sub>4</sub> NPs

Different zero charge points of the ZnFe<sub>2</sub>O<sub>4</sub> and chitosan/ZnFe<sub>2</sub>O<sub>4</sub> particles indicate composite formation. The zero charge points of chitosan/ZnFe<sub>2</sub>O<sub>4</sub> NPs show that the composite particles are negatively charged in the physiological environment (pH = 7.4). The reason for the homogeneous distribution of the particles and the absence of any aggregation observed in the experiments is that the charged composite material particles repel each other in the physiological environment and provide a stable dispersion.

### Drug loading

The maximum absorption wavelength for imatinib was determined over the range of 200 nm to 350 nm (Fig. 6a). The absorbance of imatinib was measured at 266 nm, and a calibration curve was constructed to determine the imatinib concentration encapsulated into chitosan/ZnFe<sub>2</sub>O<sub>4</sub> nanocomposite (Fig. 6b). According to the determined imatinib concentration, the encapsulation efficiency of chitosan NPs was calculated as 32.3% ± 2.1. Whereas chitosan/ZnFe<sub>2</sub>O<sub>4</sub> nanocomposite encapsulated the imatinib with an efficiency of 74.3% ± 3.8. Since imatinib was loaded to the chitosan/ZnFe<sub>2</sub>O<sub>4</sub> nanocomposite more than two times compared to the chitosan NPs, the release study of imatinib was carried out with chitosan/ZnFe<sub>2</sub>O<sub>4</sub> nanocomposite.

### *In vitro* release study of imatinib

Since the main transport of the drug will be in the physiological environment with blood, the *in vitro* drug release experiment was conducted at pH 7.4. The *in vitro* release of imatinib-loaded chitosan/ZnFe<sub>2</sub>O<sub>4</sub> nanocomposite is presented in Figure 7. The release was calculated as the cumulative amount provided up to each specified time point. Imatinib was rapidly released during the first hour and 53% of the loaded drug was released within one hour.

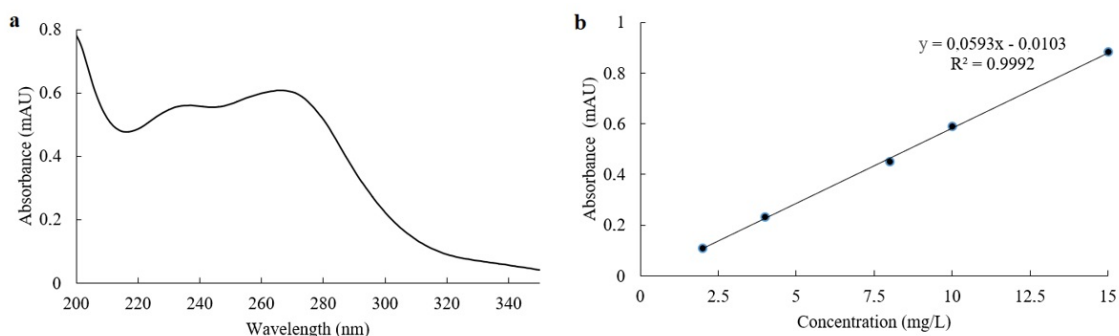


Figure 6: (a) UV spectrum and (b) Standard calibration curve of imatinib mesylate

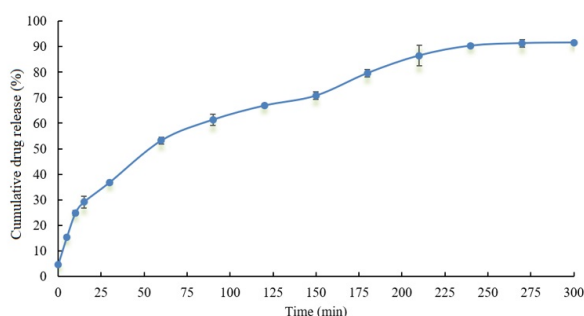


Figure 7: Cumulative drug release profile of imatinib from chitosan/ZnFe<sub>2</sub>O<sub>4</sub> nanocomposite

This rapid initial drug release for the first hour could be due to the well-known burst effect, which results from some drug quantities being localized on the surface of the nanocomposite and easily released by diffusion.<sup>46</sup> After the initial rapid release, a slower release profile of imatinib was observed between 2 and 5 hours. A sustained release curve of imatinib with nearly 91.6% of the drug released after five hours. The release profile is compatible with polymer-coated NPs given in the literature for imatinib.<sup>34,37</sup> In the study of Karimi-Ghezeli *et al.* (2019), only 40% of imatinib was released in 120 minutes from Fe<sub>3</sub>O<sub>4</sub>-chitosan NPs.<sup>38</sup> Since the nanocomposite showed almost a full release profile in our study, it could be

suggested as a delivery system for anticancer agents.

#### ***In vitro* release kinetics and release mechanism**

The correlation coefficients and the rate constants were investigated for the different kinetic models of the chitosan/ZnFe<sub>2</sub>O<sub>4</sub> nanocomposite. The data obtained from the mathematical models are listed in Table 2. The slopes of the lines correspond to the release rate constants ( $k$ ) in the zero-order and Higuchi models, while the value for  $k$  in the first-order model was obtained from the equation: slope =  $-k/2.303$ . The value of the release exponent ( $n$ ) is related to the slope of the line in the Korsmeyer-Peppas model.

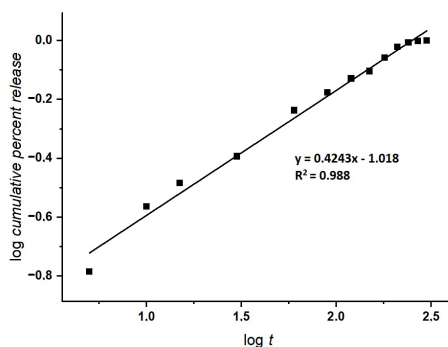


Figure 8: Korsmeyer-Peppas model for the mechanism of drug release

Table 2  
Release kinetic parameters calculated

Mathematical model	Correlation coefficient ( $R^2$ )	$k_0$ ( $\text{min}^{-1}$ )	$k_0$ ( $\text{min}^{-1}$ )	$k_H$ ( $\text{min}^{-1}$ )	n	$k_{KP}$ ( $\text{min}^{-1}$ )
Zero order	0.889	$1.63 \cdot 10^{-4}$				
First order	0.625		$8.08 \cdot 10^{-3}$			
Higuchi's model	0.880			$3.28 \cdot 10^{-4}$		
Korsmeyer-Peppas	0.988				$4.24 \cdot 10^{-1}$	$9.59 \cdot 10^{-2}$

The release kinetics of the chitosan/ZnFe<sub>2</sub>O<sub>4</sub> nanocomposite showed the highest linearity ( $R^2 = 0.988$ ) in fitting Korsmeyer-Peppas model kinetics. Figure 8 shows the linear regression graph corresponding to Korsmeyer-Peppas model.

Korsmeyer-Peppas is a simple model known as "Power law", describing drug release from a polymeric system. Korsmeyer-Peppas model describes some release mechanisms simultaneously, such as the diffusion of water into the matrix, swelling of the matrix, and dissolution of the matrix.<sup>47</sup> The release exponent of the Korsmeyer-Peppas (n) indicates the mechanisms to describe how the active compound is released from their matrix. Since it is under the value of 0.5, the solvent diffusion is much greater than the process of polymeric chain relaxation. Thus, the kinetics of this phenomenon are characterized by diffusivity.<sup>48</sup>

## CONCLUSION

In this study, the chitosan/ZnFe<sub>2</sub>O<sub>4</sub> nanocomposite was successfully prepared. FTIR spectroscopy was used to provide insight into the chemical composition of the composite nanoparticles synthesized. The morphological properties and chemical composition were determined by FESEM and EDX, respectively. Imatinib was encapsulated into the synthesized nanocomposite. The nanocomposite provided a high drug-loading capacity. Imatinib was released from the chitosan/ZnFe<sub>2</sub>O<sub>4</sub> nanocomposite into PBS buffer and showed a drug release for up to 5 h. Based on the findings, we conclude that the synthesized nanocomposite system showed potential as a delivery system for imatinib. It could be applied to lessen the adverse effects of conventional chemotherapy.

**ACKNOWLEDGMENTS:** The research was done at Istanbul Technical University (ITU), Capillary Electrophoresis, and Biopolymer Applications Research Laboratory. The authors thank METU Central Laboratory for FE-SEM and EDX analyses, and ITU for XRD analyses. The authors

thank the Research Foundation of Istanbul Technical University for the financial support (Project no: 43349).

## REFERENCES

- International Agency for Research on Cancer, Globocan 2020, accessed via Global Cancer Observatory (accessed August 2023)
- U. Anand, A. Dey, A. K. S. Chandel, R. Sanyal, A. Mishra *et al.*, *Genes. Dis.*, **10**, 1367 (2023), <https://doi.org/10.1016/j.gendis.2022.02.007>
- J. Li, S. Wang, F. Fontana, C. Tapeinos, M. A. Shahbazi *et al.*, *Bioact. Mater.*, **23**, 471 (2023), <https://doi.org/10.1016/j.bioactmat.2022.11.013>
- A. Roy and S. D. Li, *WIREs Nanomed. Nanobiotechnol.*, **8**, 891 (2016), <https://doi.org/10.1002/wnan.1406>
- S. Moradi, M. Taran, P. Mohajeri, K. Sadrjavadi, F. Sarrami, *et al.*, *J. Mol. Liq.*, **262**, 204 (2018), <https://doi.org/10.1016/j.molliq.2018.04.089>
- G. López-Pérez, R. Prado-Gotor, J. A. Fuentes-Rojas and M. J. Martín-Valero, *J. Mol. Liq.*, **302**, 112381 (2020), <https://doi.org/10.1016/j.molliq.2019.112381>
- O. R. Guadarrama-Escobar, P. Serrano-Castañeda, E. Anguiano-Almazán, A. Vázquez-Durán, M. C. Peña-Juárez *et al.*, *Int. J. Mol. Sci.*, **24**, 4289 (2023) <https://doi.org/10.3390/ijms24054289>
- S. Sharma, M. Bhende and A. Goel, *Polym. Bull.*, **81**, 8573 (2024), <https://doi.org/10.1007/s00289-023-05130-8>
- L. Alupej, G. Lisa, A. Butnariu, J. Desbrieres, A. N. Cadinoiu *et al.*, *Cellulose Chem. Technol.*, **51**, 631 (2017), [http://www.cellulosechemtechnol.ro/pdf/CCT7-8\(2017\)/p.631-649.pdf](http://www.cellulosechemtechnol.ro/pdf/CCT7-8(2017)/p.631-649.pdf)
- S. Khaledian, D. Kahrizi, S. Moradi and F. Martinez, *J. Mol. Liq.*, **334**, 116075 (2021), <https://doi.org/10.1016/j.molliq.2021.116075>
- E. Alfaro-Viquez, D. Esquivel-Alvarado, S. Madrigal-Carballo, C. G. Krueger and J. D. Reed, *Int. J. Biol. Macromol.*, **162**, 1500 (2020), <https://doi.org/10.1016/j.ijbiomac.2020.07.213>
- Ü. H. Erol, E. Güncüm and N. Işıklan, *Int. J. Biol. Macromol.*, **246**, 125627 (2023), <https://doi.org/10.1016/j.ijbiomac.2023.125627>

- <sup>13</sup> Y. Herdiana, N. Wathoni, S. Shamsuddin, I. Joni and M. Muchtaridi, *Polymers*, **13**, 1717 (2021), <https://doi.org/10.3390/polym13111717>
- <sup>14</sup> H. Choukaife, S. Seyam, B. Alallam, A. A. Doolaanea and M. Alfatama, *Int. J. Nanomed.*, **17**, 3933 (2022), <https://doi.org/10.2147/IJN.S375229>
- <sup>15</sup> S. K. Dubey, T. Bhatt, M. Agrawal, R. N. Saha, S. Saraf *et al.*, *Int. J. Biol. Macromol.*, **194**, 521 (2022), <https://doi.org/10.1016/j.ijbiomac.2021.11.095>
- <sup>16</sup> I. Z. Kuzminac, A. S. Čelić, S. S. Bekić, V. Kojić, M. P. Savić *et al.*, *Colloids Surf. B Biointerfaces*, **216**, 112597 (2022), <https://doi.org/10.1016/j.colsurfb.2022.112597>
- <sup>17</sup> E. M. Khalaf, N. A. Abood, R. Z. Atta, A. A. Ramirez-Coronel, R. Alazragi *et al.*, *Int. J. Biol. Macromol.*, **231**, 123354 (2023), <https://doi.org/10.1016/j.ijbiomac.2023.123354>
- <sup>18</sup> H. A. Asal, K. R. Shoueir, M. A. El-Hagrasy and E. A. Toson, *Int. J. Biol. Macromol.*, **209**, 2188 (2022), <https://doi.org/10.1016/j.ijbiomac.2022.04.200>
- <sup>19</sup> M. J. Sharifi, A. Nouralishahi, A. Hallajisani and M. Askari, *Cellulose Chem. Technol.*, **55**, 185 (2021), <https://doi.org/10.35812/CelluloseChemTechnol.2021.55.20>
- <sup>20</sup> M. M. Aljohani, A. Abu-Rayyan, N. H. Elsayed, F. A. Alatawi, M. Al-Anazi *et al.*, *Int. J. Biol. Macromol.*, **235**, 123704 (2023), <https://doi.org/10.1016/j.ijbiomac.2023.123704>
- <sup>21</sup> J. K. K. Alkhafagi, M. H. Tabrizi and M. Ghobeh, *J. Polym. Environ.*, **31**, 4410 (2023), <https://doi.org/10.1007/s10924-023-02904-z>
- <sup>22</sup> Z. Kalaycıoğlu, N. Kahya, V. Adımcılar, H. Kaygusuz, E. Torlak *et al.*, *Eur. Polym. J.*, **133**, 109777 (2020), <https://doi.org/10.1016/j.eurpolymj.2020.109777>
- <sup>23</sup> E. Kızılkonca, E. Torlak and F. B. Erım, *Int. J. Biol. Macromol.*, **177**, 351 (2021), <https://doi.org/10.1016/j.ijbiomac.2021.02.139>
- <sup>24</sup> N. Kahya and F. B. Erım, *Int. J. Biol. Macromol.*, **242**, 124595 (2023), <https://doi.org/10.1016/j.ijbiomac.2023.124595>
- <sup>25</sup> Z. Kalaycıoğlu, B. Özüğür-Uysal, Ö. Pekcan and F. B. Erım, *ACS Omega*, **8**, 13004 (2023), <https://doi.org/10.1021/acsomega.3c00198>
- <sup>26</sup> G. Kasparis, A. P. Sangnier, L. Wang, C. Efstathiou, A. P. LaGrow *et al.*, *J. Mater. Chem. B*, **11**, 787 (2023), <https://doi.org/10.1039/d2tb01338j>
- <sup>27</sup> C. H. Lu and J. K. Hsiao, *Tzu Chi Med. J.*, **35**, 11 (2023), [https://doi.org/10.4103/tcmj.tcmj\\_65\\_22](https://doi.org/10.4103/tcmj.tcmj_65_22)
- <sup>28</sup> J. Nowak-Jary and B. Machnicka, *Int. J. Nanomed.*, **18**, 4067 (2023), <https://doi.org/10.2147/IJN.S415063>
- <sup>29</sup> S. A. S. Shandiz, M. S. Ardestani, D. Shahbazzadeh, A. Assadi, R. A. Cohan *et al.*, *Artif. Cells Nanomed. Biotechnol.*, **45**, 1082 (2017), <https://doi.org/10.1080/21691401.2016.1202257>
- <sup>30</sup> Y. Naito, T. Nishida and T. Doi, *Gastric Cancer*, **26**, 339 (2023), <https://doi.org/10.1007/s10120-023-01381-6>
- <sup>31</sup> F. Duffaud and A. Le Cesne, *Targ. Oncol.*, **4**, 45 (2009), <https://doi.org/10.1007/s11523-008-0101-x>
- <sup>32</sup> A. Dikpati, A. Madgulkar, S. J. Kshirsagar, M. Bhalekar and A. S. Chahal, *JAPS J.*, **2**, 179 (2012)
- <sup>33</sup> I. E. Palamà, A. M. Coluccia and G. Gigli, *Nanomedicine*, **9**, 2087 (2014), <https://doi.org/10.2217/nmm.13.147>
- <sup>34</sup> S. Labala, P. K. Mandapalli, A. Kurumaddali and V. V. Venuganti, *Mol. Pharm.*, **12**, 878 (2015), <https://doi.org/10.1021/mp5007163>
- <sup>35</sup> Z. Yan, Z. Zhang and J. Chen, *Sens. Actuat. B*, **225**, 469 (2016), <https://doi.org/10.1016/j.snb.2015.10.107>
- <sup>36</sup> A. Azadpour, S. Hajrasouliha and S. Khaleghi, *J. Drug Deliv. Sci. Technol.*, **74**, 103554 (2022), <https://doi.org/10.1016/j.jddst.2022.103554>
- <sup>37</sup> S. Kalani, E. Moniri, S. A. Alavi and R. Safaeijavan, *Polym. Bull.*, **81**, 1229 (2024), <https://doi.org/10.1007/s00289-023-04760-2>
- <sup>38</sup> Z. Karimi Ghezeli, M. Hekmati and H. Veisi, *Appl. Organometal. Chem.*, **33**, e4833 (2019), <https://doi.org/10.1002/aoc.4833>
- <sup>39</sup> S. Tuna, A. Beyler-Cigil and S. Demir, *Cellulose Chem. Technol.*, **56**, 795 (2022), <https://doi.org/10.35812/CelluloseChemTechnol.2022.56.71>
- <sup>40</sup> P. Calvo, C. Remuñan-Lopez, J. L. Vila-Jato and M. J. Alonso, *J. Appl. Polym. Sci.*, **63**, 125 (1998), [https://doi.org/10.1002/\(SICI\)1097-4628\(19970103\)63:1<125::AID-APP13>3.0.CO;2-4](https://doi.org/10.1002/(SICI)1097-4628(19970103)63:1<125::AID-APP13>3.0.CO;2-4)
- <sup>41</sup> R. Jalababu, S. Satya Veni and K. V. N. Suresh Reddy, *J. Drug Deliv. Sci. Technol.*, **44**, 190 (2018), <https://doi.org/10.1016/j.jddst.2017.12.013>
- <sup>42</sup> E. Bellur Atici and B. Karliğa, *J. Pharm. Biomed. Anal.*, **114**, 330 (2015), <https://doi.org/10.1016/j.jpba.2015.06.011>
- <sup>43</sup> M. X. Lin, Y. Wu and S. Rohani, *J. Cryst. Growth*, **507**, 146 (2019), <https://doi.org/10.1016/j.jcrysgro.2018.10.061>
- <sup>44</sup> W. Szczepek, D. Samson-Lazinska, B. Zagrodzki, M. Glice, W. Maruszak *et al.*, U.S. Patent 7, 732, 601 (2010)
- <sup>45</sup> A. E. Abdelhamid, E. H. Ahmed, H. M. Awad and M. M. H. Ayoub, *Polym. Bull.*, **81**, 1421 (2024), <https://doi.org/10.1007/s00289-023-04768-8>
- <sup>46</sup> J. Supramaniam, R. Adnan, N. H. M. Kaus and R. Bushra, *Int. J. Biol. Macromol.*, **118**, 640 (2017), <https://doi.org/10.1016/j.ijbiomac.2018.06.043>
- <sup>47</sup> M. L. Bruschi, "Strategies to Modify the Drug Release from Pharmaceutical Systems", Woodhead Publishing, Elsevier, 2015, p. 64, <https://doi.org/10.1016/C2014-0-02342-8>
- <sup>48</sup> S. C. Basak, K. S. Kumar and M. Ramalingam, *Brazil. J. Pharm. Sci.*, **44** (2008)